R. Saito[1)], A. Jorio[2)], J. Jiang[3)], G. Dresselhaus[4)], and M. S. Dresselhaus[4)]

[1)]Tohoku University, Sendai, Japan
[2)]Univerisidade Federal de Minas Gerais, Belo Horizonte, Brazil
[3)]North Carolina State University, Rayleigh, NC, USA
[4)]Massachusetts Institute of Technology, Cambridge, MA 02139, USA

OPTICAL PROPERTIES OF CARBON NANOTUBES AND NANO-GRAPHENE

R. Saito, A. Jorio, J. Jiang, G. Dresselhaus, and M. S. Dresselhaus

1 OVERVIEW

1.1 Shape of graphene and nanotubes

Graphene (GR) is a single planar sheet of a hexagonal lattice of graphite[1]. A single wall carbon nanotube (SWNT) is a monolayer graphene sheet rolled up into a cylinder (Iijima, 1991, Saito *et al.*, 1998a, Jorio *et al.*, 2007). When the constituent graphene sheets are two (many), GR and SWNT become bilayer graphene (graphite) and double (or multi) wall carbon nanotubes (DWNTs, MWNTs). Carbon nanotubes and graphene are now widely investigated as nano-materials since the thickness of a graphene sheet or the diameter of a carbon nanotube is on the order of a nano-meter. When we put electrodes at both ends of a GR or a SWNT with a gate electrode in between, we can make a semiconductor device. A graphene sheet possesses many unique transport (Zhang *et al.*, 2005, Novoselov *et al.*, 2005), mechanical, and optical properties (Pimenta *et al.*, 2007). Thus in order to get the high performance that these materials can provide, we should know how to evaluate the sample. Especially for carbon nanotubes, depending on how we roll the GR sheet, there are more than 200 different geometrical structures that a SWNT can assume, which we call the SWNT chirality (Saito *et al.*, 1998a). An important finding of SWNTs is that the electronic properties of a SWNT can be either metallic or semiconducting depending on the chirality (Saito *et al.*, 1992b, Hamada *et al.*, 1992, Saito

[1] A graphene ribbon is a graphene sheet with a finite width in one direction in the plane.

et al., 1992a, Tanaka *et al.*, 1992). Thus the electronic properties of either semiconducting or metallic materials can be obtained only by changing the chirality.

1.2 Raman Spectroscopy

In the following, starting from the basic definition of a carbon nanotube and graphene, we will show the basic concepts behind graphene and SWNTs. The structure of a SWNT can be seen by many spectroscopic techniques, such as resonance Raman spectroscopy, electron diffraction, and scanning probe microscopy (SPM) (Jorio *et al.*, 2007). Among them, resonance Raman spectroscopy is widely used by many groups for nanotube characterization since Raman spectroscopy is a non-destructive, non-contact measurement that is carried out under ambient air pressure and room temperature (Rao *et al.*, 1997, Doorn *et al.*, 2003, Fantini *et al.*, 2004, Telg *et al.*, 2004). Using an optical microscope, the excitation laser light can be focused down to the wavelength of the light, and thus a spatial resolution up to 1 μm can be obtained, which we call confocal micro-Raman spectroscopy. When the excitation energy is equal to the transition energy of the materials, the Raman signal is enhanced significantly (say by an order of 1000) and this is known as resonance Raman spectroscopy. Thus if we use many laser excitation energies, we can plot the Raman intensity as a function of laser excitation energy, which we call the Raman excitation profiles, from which we gain information about the transition energy of each unique SWNT (Doorn *et al.*, 2003, Fantini *et al.*, 2004, Telg *et al.*, 2004).

In graphene and SWNTs, a strong Raman-active mode is the so-called G-band appearing at around 1580-1595 cm^{-1} (Dresselhaus *et al.*, 2005, Jorio *et al.*, 2003a). The G-band in graphene is an optic phonon mode in which the longitudinal optic (LO) and transverse optic (TO) phonon modes are degenerate. In the case of SWNTs, these two G-band phonon modes are split mainly into two which we call G^+ and G^-, whose frequency separation is proportional to the inverse of the square of the diameter (Jorio *et al.*, 2002). Group theory tells us that the Raman-active modes of SWNTs have A, E_1 and E_2 symmetries for the rotational symmetry around the nanotube axis, and only the A modes have a strong intensity (Saito *et al.*, 2001, Jorio *et al.*, 2000). Around 1350 cm^{-1}, we can see the D-band phonon mode whose intensity depends on the amount of defect structure in the SWNTs (Pimenta *et al.*, 2007). The D-band and G-band intensity ratio is proportional to $1/L_a$ (the crystalline size) (Tuinstra and Koenig, 1970a,b) and to $1/E_{\mathrm{laser}}^4$ (where E_{laser} denotes the laser excitation energy) (Sato *et al.*, 2006, Cancado *et al.*, 2006). One important issue for the D-band is its dispersions, whereby the frequency of the D-band increases by 53 cm^{-1}/eV with increasing E_{laser} (Matthews *et al.*, 1999). SWNTs have a radial breathing mode (RBM) in which the C atoms along the diameter of the SWNT are vibrating coherently in the radial direction. The frequency of the RBM ω_{RBM} is inversely proportional to the diameter d_t. There are many important Raman modes appearing between 100 and 3200 cm^{-1} (Dresselhaus *et al.*, 2005, Jorio *et al.*, 2003a). If the reader knows the characteristics of each phonon mode, the information provided by Raman spectroscopy is very rich, and thus the Raman spectroscopy of graphene and SWNTs have become a standard for characterizing such samples.

1.3 Exciton physics

When we discuss an optical process for SWNTs, an exciton (a bound pair of a photo-excited electron and a hole) is important (Ando, 1997, Pedersen, 2003, Spataru *et al.*, 2004, Zhao and Mazumdar, 2005, Dresselhaus *et al.*, 2007). In conventional semiconductors, an exciton exists only at low temperature below 10K. Since the exciton binding energy for a SWNT is very large up to 1 eV because of the low dimensionality of the SWNT, an exciton can exist even at room temperature. Thus the energy gap for a single particle (transport) and the optical transition energy for an exciton are different from each other because of many body effects (Dresselhaus *et al.*, 2007). Because of the localization of the wave-function in real space, the delocalized Bloch wave-functions labeled by the wave-vector k are mixed with each other by the Coulomb interaction, and we solve for the mixing term by the Bethe–Salpeter equation (Jiang *et al.*, 2007a). Since an electron or a hole can exist on one of the two energy dispersion curves around the degenerate Fermi energy, there are four possibilities (16 if we include spin) for the excitonic states[2]. Because of the symmetry, three of the four excitonic states are not optically allowed and we call them dark excitons and only one of the four excitons is optically allowed (a bright exciton) (Barros *et al.*, 2006b,a). Since one of the dark exciton states has a smaller transition energy than the bright exciton state, the quantum efficiency of SWNTs cannot be so high[3]. In Section 5 we will discuss how to calculate the excitonic states and their relationship to resonance Raman spectroscopy for SWNTs.

2 DEFINITION OF CARBON NANOTUBES AND NANO-GRAPHENE

2.1 Crystal structure of graphene

The crystal structure of monolayer graphene is a two-dimensional hexagonal sheet (Saito *et al.*, 1998a). The bond length of the two nearest neighbor carbon atoms is 1.42 Å. We define the unit vectors $\boldsymbol{a}_1$ and $\boldsymbol{a}_2$ as shown in Fig. 1, whose lengths are each 1.42 Å$\times\sqrt{3}$=2.46 Å. The unit cell of graphene is given by a rhombus (or a hexagon) containing two carbon atoms (A and B). The corresponding reciprocal lattice is obtained by rotating the hexagonal lattice in real space by 90 degrees and the reciprocal lattice vectors are given by $\boldsymbol{b}_1$ and $\boldsymbol{b}_2$ in Fig. 1(b). Thus the first Brillouin zone is a hexagon in k space and Γ, K and M denote symmetrical points in the 2D Brillouin zone, respectively, at zone center, hexagonal corner, and the center of the edge.

A carbon atom has atomic orbitals 1s, 2s, 2p in which the 2s and in-plane $2p_x$ and $2p_y$ orbitals hybridize with one another to make a covalent bond (σ bond) between the three nearest neighbor carbon atoms, forming the strongest chemical bond among materials. The remaining $2p_z$ orbitals make a π bond to each other to form the valence electrons. The π energy band consists of the two $2p_z$ orbitals of the A and B atoms in the unit cell. Using a simple tight binding model, the Hamiltonian matrix, $\mathcal{H}$ and the overlap matrix $\mathcal{S}$ are given by 2×2 matrices:

[2]In the case of an armchair nanotube, since there are two energy minima in the 1D Brillouin zone, we have 16 possible pairs of excitons without considering spin.

[3]The energy separation between the dark and the bright excitons states are smaller than the thermal energy at room temperature. Thus we expect a reasonable population of bright exciton states at room temperature. However, since the dark exciton states increase the number of phonon-emission processes, the quantum efficiency is low.

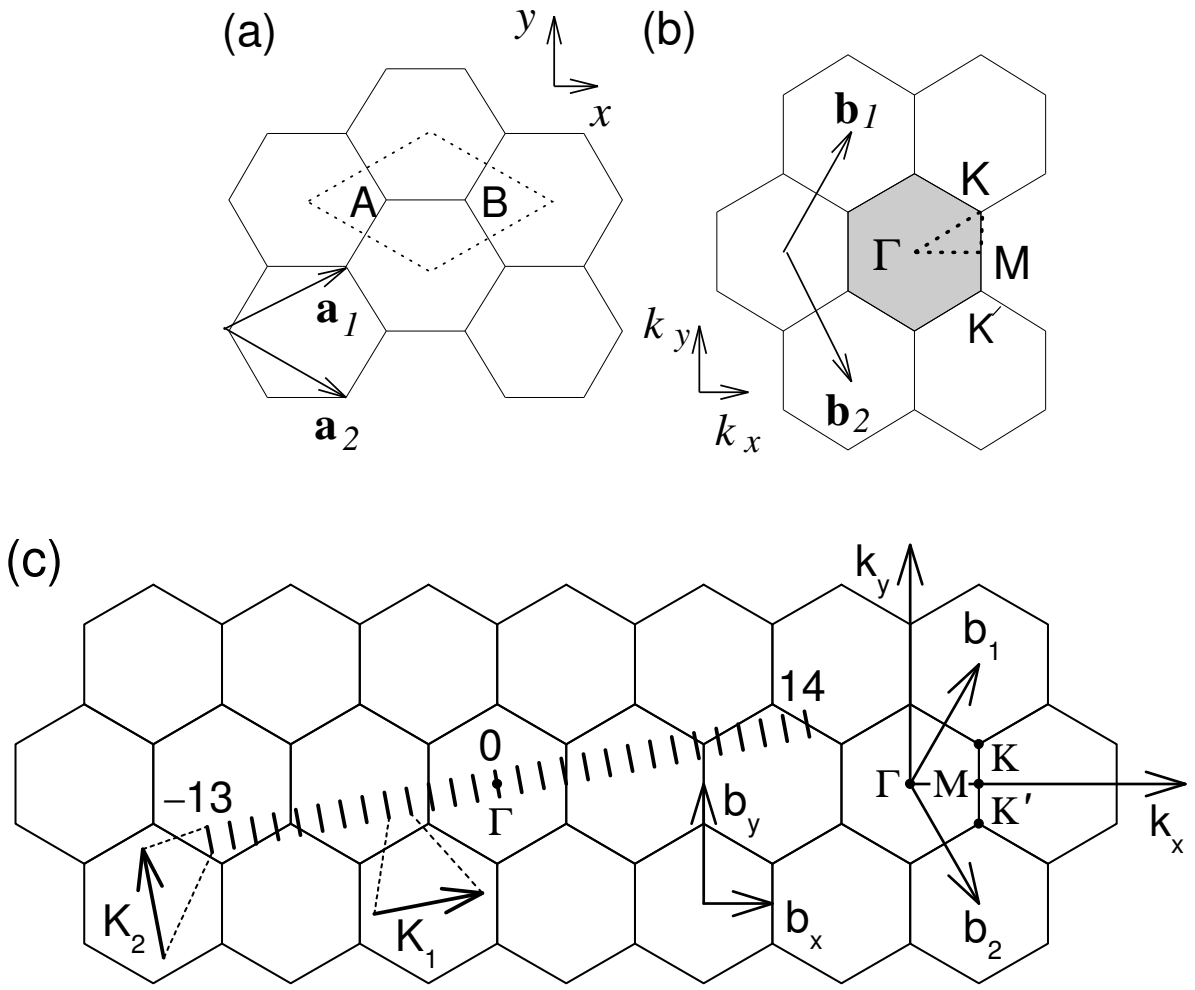

Figure 1: (a) The unit cell and (b) Brillouin zone of graphene are shown as the dotted rhombus and the shaded hexagon, respectively. $\vec{a}_i$, and $\vec{b}_i$, $(i = 1, 2)$ are unit vectors and reciprocal lattice vectors, respectively. (c) Parallel equidistant lines represent the cutting lines for the $(4, 2)$ nanotube. The cutting lines are labeled by the cutting line index μ, which assumes integer values from $1 - N/2 = -13$ to $N/2 = 14$ (Saito *et al.*, 1998a).

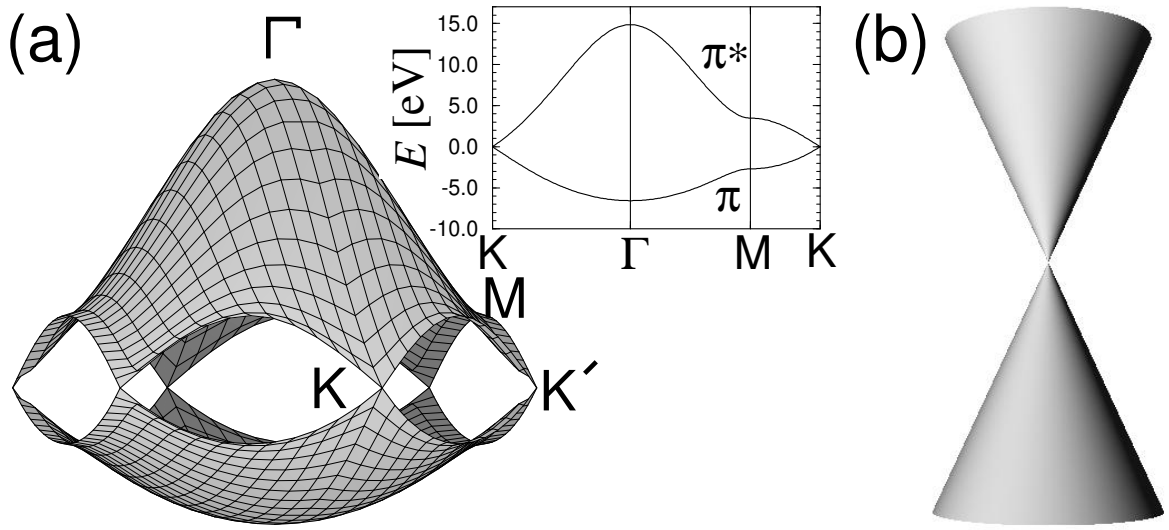

Figure 2: (a) The energy dispersion relations for 2D graphite are shown throughout the whole region of the Brillouin zone. The inset shows the energy dispersion along the high symmetry directions of the triangle ΓMK shown in Fig. 1(b) (see text). (b) Around the K (or K′) point, the energy dispersion is expressed by two cones (the Dirac cones).

$$\mathcal{H} = \begin{pmatrix} \epsilon_{2p} & tf(k) \\ tf(k)^* & \epsilon_{2p} \end{pmatrix}, \quad \mathcal{S} = \begin{pmatrix} 1 & sf(k) \\ sf(k)^* & 1 \end{pmatrix}. \tag{1}$$

where γ_0 and s are, respectively, the nearest neighbor hopping and overlap integrals between A and B atoms and $f(x)$ is the phase factor appearing in the Bloch wave-function consisting of A and B atoms.

$$f(k) = e^{ik_x a/\sqrt{3}} + 2e^{-ik_x a/2\sqrt{3}} \cos\left(\frac{k_y a}{2}\right). \tag{2}$$

Solving the secular equation $\det(\mathcal{H} - E\mathcal{S}) = 0$, the energy band $E(\vec{k})$ is obtained as a function of $w(\vec{k})$, k_x and k_y:

$$E_{g2D}(\vec{k}) = \frac{\epsilon_{2p} \pm tw(\vec{k})}{1 \pm sw(\vec{k})}, \tag{3}$$

where the function $w(\vec{k})$ is given by:

$$w(\vec{k}) = \sqrt{|f(\vec{k})|^2} = \sqrt{1 + 4\cos\frac{\sqrt{3}k_x a}{2}\cos\frac{k_y a}{2} + 4\cos^2\frac{k_y a}{2}}. \tag{4}$$

The π energy bands consist of an occupied π band and an unoccupied π^* band whose energy gap at the K point is zero. The energy band width for the π^* band is larger than that for

the π band because of the s parameter. The energy dispersion near the K point is linear around the K point, and thus the energy bands near the Fermi energy $E_{\rm F}$ at the K point have two cones whose apexes touch each other (see Fig. 2(b)). Near $E_{\rm F}$, we have two sets of cones, one set around the K point and the other around the K$'$ point. Thus the energy is always degenerate for k and $-k$ states (due to time reversal symmetry).

2.2 Electronic structure of SWNTs

When we unroll a SWNT, we get a graphene sheet with a fixed width (nano graphene ribbon). Thus when we neglect the curvature effect of the cylinder, the electronic structure of the nano-graphene and a SWNT are the same, except for the electronic states at the edges of the graphene. In the equatorial direction, there is a periodicity which connects the same atom by a vector around the equator of the cylinder, which we call a chiral vector, $\boldsymbol{C}_h = n\boldsymbol{a}_1 + m\boldsymbol{a}_2 \equiv (n, m)$. The diameter of a nanotube is given by $d_t = |\boldsymbol{C}_h|/\pi = a\sqrt{n^2 + m^2 + nm}$. In the direction of the nanotube axis, there is a periodicity of $\boldsymbol{T}$ which is perpendicular to $\boldsymbol{C}_h$; and $\boldsymbol{T} = t_1\boldsymbol{a}_1 + t_2\boldsymbol{a}_2 \equiv (t_1, t_2)$, where t_1, and t_2 are given by $t_1 = (2m + n)/d_R$, and $t_2 = -(2n + m)/d_R$ with $d_R = \gcd(2m + n, 2n + m)$ (gcd = the greatest common divisor of two integers). The unit cell of a SWNT is a rectangle specified by $\boldsymbol{C}_h$ and $\boldsymbol{T}$, in which we have $N \equiv 2(m^2 + n^2 + nm)/d_R$ hexagon and $2N$ carbon atoms. Thus we will get $2N$ one-dimensional (1D) energy bands (Saito *et al.*, 1998a).

The reciprocal lattice vectors of a SWNT for $\boldsymbol{C}_h$ and $\boldsymbol{T}$ are, respectively, $\boldsymbol{K}_1$ and $\boldsymbol{K}_2$, where $\boldsymbol{K}_1 = (-t_2\boldsymbol{b}_1 + t_1\boldsymbol{b}_2)/N$ and $\boldsymbol{K}_2 = (m\boldsymbol{b}_1 - n\boldsymbol{b}_2)/N$. We have N discrete values of k_c in the direction of $\boldsymbol{K}_1$, ($\mu\boldsymbol{K}_1, \mu = 1, \ldots N$) and a continuous value of k is taken in the direction of $\boldsymbol{K}_2$, $-\pi/T < k < \pi/T$ (see Fig. 1(b)). When we plot the possible k values in the 2D Brillouin zone, there are N line segments which we call cutting lines, separated by $|\boldsymbol{K}_1|$ with a length, $2\pi/T$. Thus the electronic energy band consists of N π and π^* energy subbands which cut the 2D energy dispersion curve of graphene in the direction of $\boldsymbol{K}_1$,

$$E_\mu(k) = E_{g2D}\left(k\frac{\boldsymbol{K}_2}{|\boldsymbol{K}_2|} + \mu\boldsymbol{K}_1\right),\ (\mu = 1, \ldots, N;\ -\frac{\pi}{T} < k < \frac{\pi}{T}). \tag{5}$$

If a μ-th cutting line goes through the K point, the SWNT energy band becomes metallic, while if no cutting line goes through the K point, the SWNT will have an energy gap (semiconducting). When we calculate the distance of $\Gamma\vec{K}$ in units of $\boldsymbol{K}_1$, we get

$$\frac{\overrightarrow{\Gamma K}\cdot\boldsymbol{K}_1}{|\boldsymbol{K}_1|^2} = \frac{2n + m}{3}. \tag{6}$$

When $2n + m = 3p + r$, (p is an integer and $r = 0, 1,$ and 2), the corresponding SWNTs are, respectively, metallic, type I semiconductor and type II semiconductor NTs. The difference between type I and type II semiconductor nanotubes is the position of the K point between two nearest cutting lines. (See Fig. 3.)

When the 1D energy subband has a minimum (or maximum), the density of states becomes singular at that energy ($\propto 1/\sqrt{E - E_0}$), and the optical absorption becomes strong at this

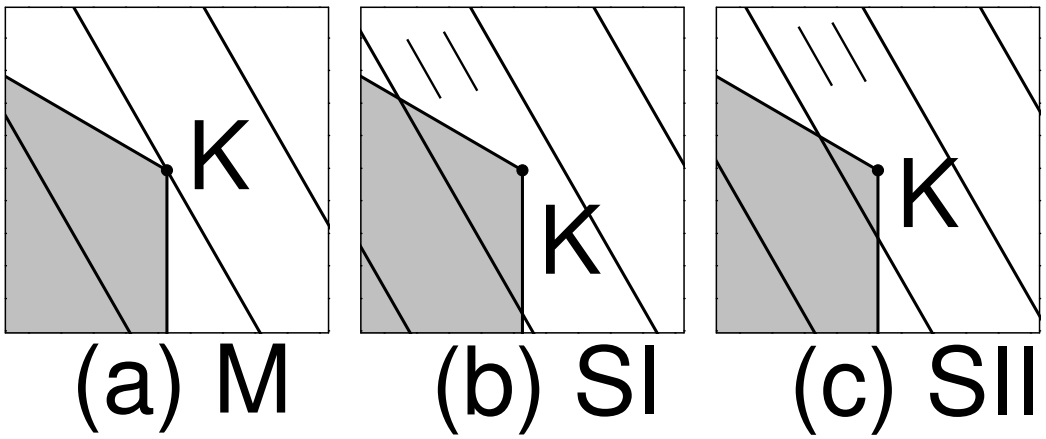

Figure 3: Cutting lines around the K point for (a) Metallic (M), (b) Type-I (SI) semiconducting, (c) Type-II (SII) semiconducting single wall carbon nanotubes. In the case of semiconducting SWNTs, the K point exists at a 2/3 or 1/3 position between two nearest cutting lines. (Saito *et al.*, 1998a, Samsonidze *et al.*, 2003)

energy[4].

3 EXPERIMENTAL SETUP FOR CONFOCAL RESONANCE RAMAN SPECTROSCOPY

The basic setup for the Raman scattering experiment is an excitation laser, a monochromator and a detector. An interference filter is needed before the sample to remove plasma lines (or luminescence) from the lasers. Another filter (a notch filter) has to be placed before the monochromator to filter the elastic scattered light. Resonance Raman spectra requires many excitation laser lines to get in and out of resonance with different SWNTs. In this case, the filters have to be tunable. The interference filter can be replaced by a set of prisms, although this is not very efficient. Alternatively, they can be replaced by another monochromator. There are already tunable notch filters available, but they are rather expensive. To filter the scattered light of a tunable system, usually researches use a triple-monochromator micro-Raman setup. The two prior gratings, usually used in the fore-monochromator stage, serve to eliminate the light originating from elastic scattering processes, and the last grating, usually called a spectrograph, is responsible for the dispersion of the light originating from the inelastic scattering.

For a one laser line experiment, a single-monochromator micro-Raman system can be used. In this case the scattered light goes directly from the sample to the spectrograph stage passing through a notch filter which blocks the elastic scattered light. A more intensive Raman signal is obtained with a single-monochromator (usually 100 times stronger).

[4]In the case of an exciton, the energy subband is as a function of the center of momentum and again we have a singular density of states at the energy minimum.

For the excitation, typically both discrete excitation energies from Ar:Kr and He:Ne lasers, and tunable Ti:Sapphire and dye lasers are used. Both Ti:Sapphire and dye lasers are usually pumped by an Ar ion laser with output power $\sim$6W. The Ti:Sapphire laser provides tunable output wavelengths in the near infra-red (NIR) range and the dye laser allows us to change the output wavelengths in the visible region and the specific wavelength range depends on the kind of dye solution used.

In micro-Raman measurements, an optical microscope is attached to the system so that we can get a spatial resolution of the order of the wavelength of light. Usually the samples are focused using $10\times$, $50\times$ and $100\times$ objectives for SWNTs in solution, in bundles and isolated on a SiO_2 substrate, respectively. In experiments with carbon nanotube samples on SiO_2 substrates or suspended in aqueous solution, high laser power density (up to 40 mW/μm^2) can be used sometimes without heating or damaging the samples. For nanotube samples in bundles or as isolated SWNTs suspended in air, a low power density ($<$1 mW/μm^2) must be used to prevent heating of the SWNTs, since the frequency and intensity of the spectral features are temperature dependent.

For polarized Raman experiments, an analyzer is placed after the microscope and two half-wave plates are placed, one before and another after the microscope, to rotate the polarization of the incident and scattered light with respect to the nanotube axis. Alternatively, only one half-wave plate that rotates both incident and scattered light beams can be used, as illustrated in Ref. (Duesberg *et al.*, 2000).

4 RAMAN SIGNALS AND SAMPLE EVALUATION

4.1 Resonance Raman spectroscopy, the Kataura plot

Stokes (or Anti-Stokes) Raman scattering is the inelastic scattering of light by emitting (or absorbing) a phonon. The optical process of Raman scattering consists of (1) photo-absorption, (2) phonon emission and (3) photo-emission. In perturbation theory, the first-order Raman intensity [see Fig. 4 (a)] as a function of phonon energy, $\hbar\omega$, and of the incident laser energy, $E_{\rm laser}$ is calculated by (Cardona, 1982, Martin and Falicov, 1983)

$$I(\omega, E_{\rm laser}) = \sum_j \left| \sum_b \frac{M^d(\boldsymbol{k}-q, jb) M^{ep}(\boldsymbol{q}, ba) M^d(\boldsymbol{k}, aj)}{\Delta E_{\rm aj}(\Delta E_{\rm aj} - \hbar\omega)} \right|^2 , \tag{7}$$

in which $\Delta E_{\rm aj} \equiv E_{\rm laser} - (E_{\rm a} - E_{\rm j}) - i\gamma$, and j, a and b denote, respectively, the initial state, the excited states, and the scattered states of an electron, while γ denotes the broadening factor of the resonance event. If photo-absorption or photo-emission occurs for a real electronic transition, the Raman intensity is enhanced significantly because one of the energy denominators in Eq. (7) becomes zero. This situation is called resonance Raman scattering and we say that the laser excitation energy is resonant with the optical transition energy. In the case of SWNTs, the joint density of states for an optical transition becomes singular (van Hove singularity), a strong enhancement of the Raman intensity occurs. Thus even for one SWNT, we can get a Raman signal if $E_{\rm laser}$ matches the optical transition energy. The optical transition energy of a SWNT is given by the exciton energy E_{ii} in which an electron in the i-th conduction band is combined

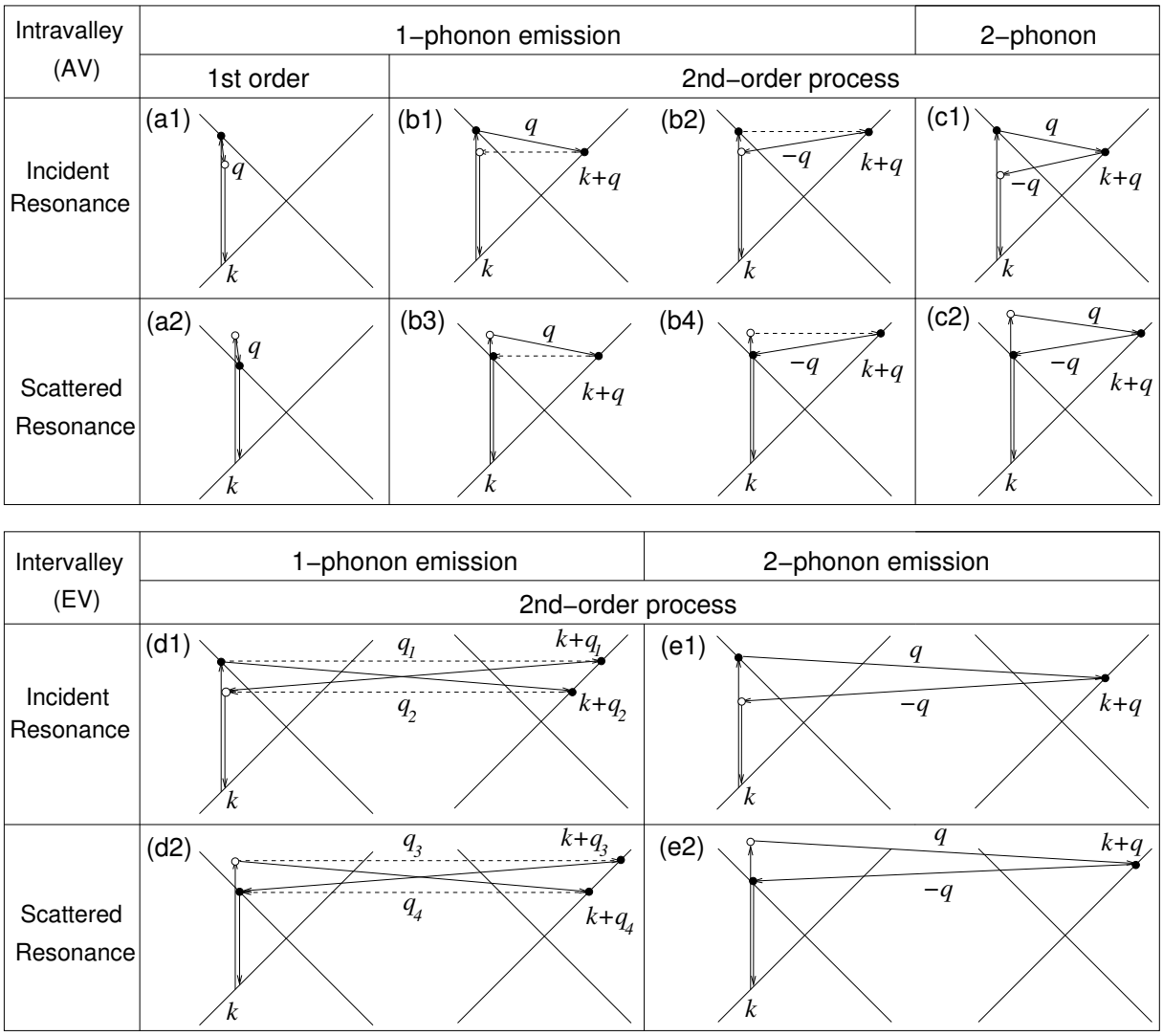

Figure 4: (up) Intravalley scattering (AV) : (a) First-order and (b) one-phonon second-order, (c) two-phonon second-order, resonance Raman spectral processes. (top) incident photon resonance and (bottom) scattered photon resonance conditions. For one-phonon, second-order transitions, one of the two scattering events is an elastic scattering event (dashed lines). Resonance points are shown as solid circles. (down) Intervalley scattering (EV) (d) one-phonon second-order, (e) two-phonon second-order, resonance Raman spectral processes. In the case of (d), depending on whether the elastic scattering occurs first or not, two possible q vectors exist. For each case, the upper (lower) row corresponds to incident (scattered) resonance conditions.

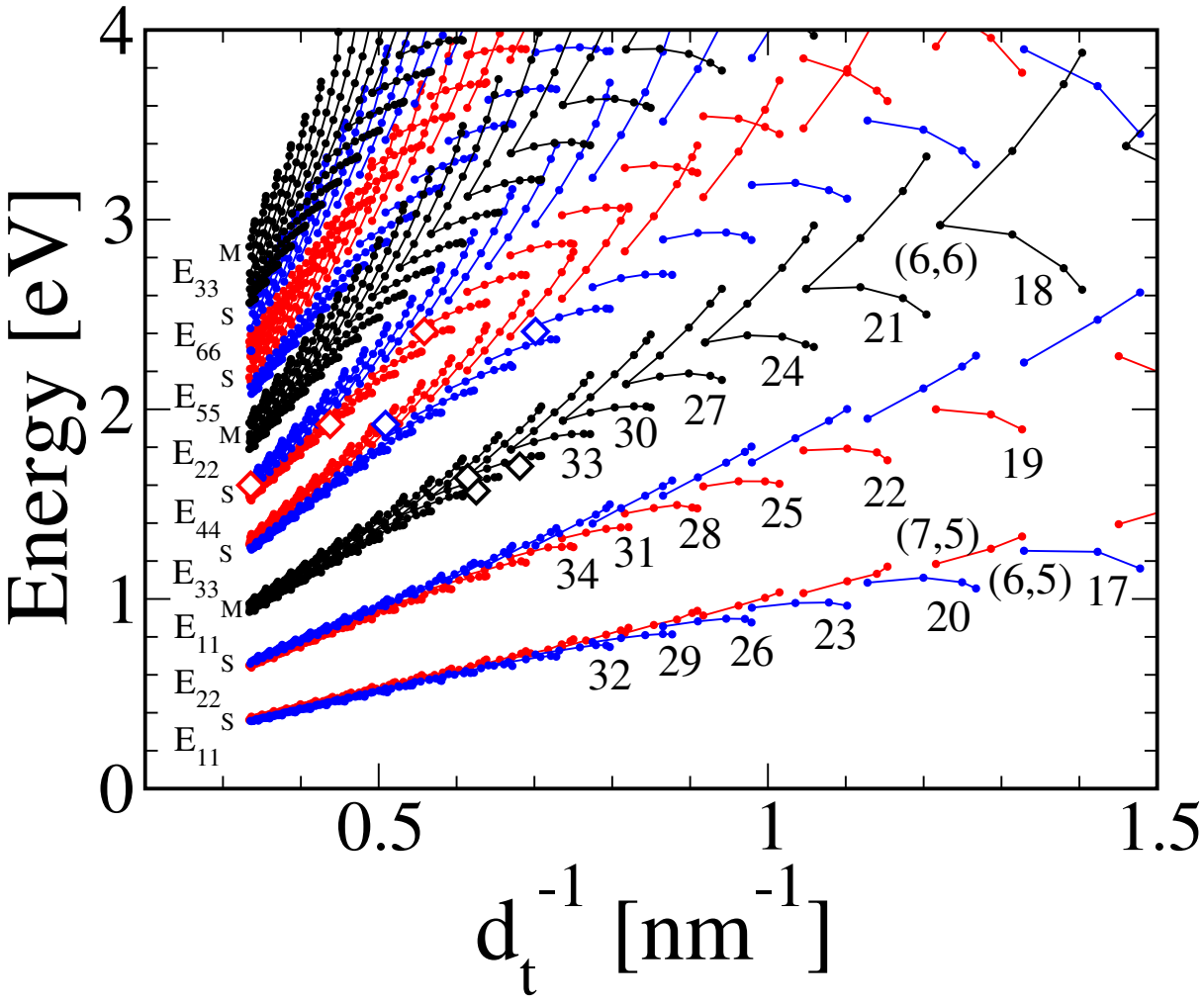

Figure 5: Kataura plot of E_{ii} for all optically allowed excitons as a function of d_t. The numbers denote $(2n+m)$ families and a few representative (n,m) nanotubes are indicated. The diamond symbols are experimental data by Sauvajol *et al.* (Sato *et al.*, 2007b)

with a hole in the i-th valence band. Originally we used this notation for the transition energy of an electron between the two energy bands (Samsonidze *et al.*, 2004). We here use this notation for the exciton formation energy.

In Fig. 5, we plot E_{ii} for all optically allowed excitons as a function of nanotube diameter d_t (the Kataura plot). Each point corresponds to a particular (n,m) SWNT, and for a given $E_{\rm laser}$ we know from Fig. 5 which (n,m) SWNT is resonant. For $d_t < 2\,$nm, only a few (n,m) can be resonant for a given laser energy. Thus combined with the fact that the RBM frequency is given by $\omega_{\rm RBM} \propto 1/d_t$, we can assign (n,m) almost uniquely from Raman spectra and using Fig. 5 (Doorn *et al.*, 2003, Fantini *et al.*, 2004, Telg *et al.*, 2004). When we change $E_{\rm laser}$ around the resonant energy, the enhancement of the Raman intensity can be seen within a small range (0.1 eV) of energy (Jorio *et al.*, 2001, Doorn *et al.*, 2003, Fantini *et al.*, 2004, Telg *et al.*, 2004).

We call this intensity change with $E_{\rm laser}$ a resonance Raman excitation profile. We have to satisfy two resonance conditions, namely the incident resonance condition ($E_{\rm laser} = E_{ii}$) and the scattered resonance condition ($E_{\rm laser} = E_{ii} + E_{\rm phonon}$). In the incident resonance condition, the excitation laser energy is equal to the optical absorption energy, and all Raman-active phonon modes are enhanced at the same time. For the scattered resonance condition, the exciton energy after losing the phonon energy is equal to $E_{\rm laser}$, in which only one specified phonon mode is resonant.

There are many known Raman modes in graphite (graphene) and SWNTs, the most important being the G-band around 1580-90 $\rm cm^{-1}$ and the radial breathing mode (RBM), the last with a predicted frequency dependence with tube diameter given by $\omega_{\rm RBM} = A/d_t$ $\rm cm^{-1}$. These are zone-centered phonons (modes at the center of the Brillouin zone) that participate in the first-order Raman scattering in all SWNTs, and the RBM has been largely used to measure the diameter distribution in a sample. The proportionality constant $A = 227\,\rm cm^{-1}\cdot nm$ is expected from elasticity theory (Mahan, 2002). However, different values are found in the literature, and most of the empirical $\omega_{\rm RBM}$ vs d_t relations reported up to now, have employed an empirical offset parameter B ($\omega_{\rm RBM} = A/d_t + B$) (Araujo *et al.*, 2007, Fantini *et al.*, 2004, Jorio *et al.*, 2001, Paillet *et al.*, 2006, Bachilo *et al.*, 2002, Hartschuh *et al.*, 2003, Telg *et al.*, 2004, Doorn *et al.*, 2004, Strano, 2003, Pfeiffer *et al.*, 2005) The B supposedly accounts for environmental effects, such as interaction between the SWNT and a substrate, surfactant, another nearby SWNT, etc. Obviously, this correctional offset contradicts the simple physical requirement of a vanishing radial breathing mode frequency as d_t approaches infinity, *i.e.* for a flat graphene sheet.

4.2 Double resonance Raman scattering

The G′ band which appears around 2700 $\rm cm^{-1}$ is a strong Raman band (especially for graphene) and is a two-phonon second-order Raman mode. In the second-order Raman spectra, we have two scattering processes. In order to recombine the photo-excited electron and a hole, the wave vector for the electron and the hole should be the same. Thus, in first-order Raman scattering, the wave-vector should be zero (zone centered phonon), while in the case of second-order Raman scattering, the wave-vectors for two phonons are relaxed to q and $-q$, and thus non-zone-centered phonon modes can be seen experimentally (Fig. 4(b)-(e)).

As for the G′ band, the phonon around the K point is relevant. In the case of second order Raman scattering, the spectra is generally weak and broad because of the many possibilities for selection of the q wave-vector. However if the two of the three energy denominators[5] becomes zero at the same time, the intensity becomes as strong as a first-order resonance Raman process. This effect is known as double-resonance Raman scattering. When the intermediate electronic states for the photo-excited electron after emitting the q phonon is a real electronic state, the double resonance condition is fulfilled when combined with satisfying either the incident photon resonance or the scattered photon resonance condition. The intermediate states are selected such that the energy-momentum condition for the scattering of an electron by a photon with momentum q and energy $\hbar\omega(q)$ is satisfied. Since there are (1) six phonon energy dispersion

[5]In the case of second-order Raman scattering, we add to Eq. (7) one more scattering matrix element in the numerator and one more energy denominator to obtain the next higher perturbation term.

branches, (2) two electronic energy dispersion relations around the K and K′ points, and (3) two possibilities for forward and backward scattering in 1D materials[6], there are 24 possible intermediate states that conserve energy-momentum in a scattering process. Among these various scattering processes, the G′ band is strong because the electron-phonon matrix element for (1) the optic phonon mode, (2) the q vector around the K′ point and (3) the backward scattering are all known to be strong by calculation (Jiang *et al.*, 2005a). The other two phonon modes are relatively weak but we can under some experimental conditions obtain enough intensity to assign some of them, and such phonons modes are listed in Table1.

4.3 Dispersion behavior of second-order Raman modes

In second order scattering, the phonon modes for q and $-q$ need not be the same. If the two phonons are the same phonon mode, we call the corresponding Raman mode an overtone mode (or harmonic), while if the two phonons are not the same, we call it a combination phonon mode. We can also include the case of $q = 0$ for overtone and combination phonon modes in which two first-order processes occur for a photo-excited electron. However a unique feature for the second-order Raman spectra is a dispersion behavior in which the observed Raman frequencies depend on $E_{\rm laser}$.

The origin of the dispersion behavior comes from the linear energy dispersion of the electronic energy around the K (K′) point (see Fig. 4). When $E_{\rm laser}$ increases, the optically allowed k vector of an electron measured from the K point also increases because it is proportional to $E_{\rm laser}$. Thus, since the backward scattering q vector is $q = 2k$ (or $q = 2k + \Gamma\vec{K}$ for scattering from the K to the K′ point in an inter-valley scattering process.), we see that the phonon frequency increases as q increases (or decreases) along the phonon dispersion with a slope $\partial\omega_q/\partial E_{\rm laser}$ for graphite or SWNTs.(Saito *et al.*, 2002).

4.4 Kohn anomaly of phonons: doping effect

When graphene, graphite or SWNTs are metallic, either as prepared or by doping, some specific phonons become soft (i.e. are strongly down shifted in frequency) by the electron-phonon interaction between phonons and nearly free electrons (or holes). (Piscanec *et al.*, 2004, Ando, 2006a, Piscanec *et al.*, 2007) The downshift of the phonon frequency is known as the Kohn anomaly, which can be of significant magnitude (say 50 cm^{-1}) in SWNTs (See, for example, Chapter by J. -C. Charlier et al. in (Jorio *et al.*, 2007). An electron with a given Fermi wave-vector $k_{\rm F}$ couples most strongly to phonons with wave-vector $q = 2k_{\rm F}$ since the corresponding susceptibility is large[7]. Since graphene and SWNTs have a Fermi surface around K and K′, the two possible conditions for $2k_{\rm F}$ are intra-valley scattering ($2k_{\rm F} \sim 0$) and inter-valley scattering ($2k_{\rm F} \sim \Gamma\vec{K}$). Thus Raman active phonon modes around both the Γ and the K points can be

[6] A Backward (forward) scattering is defined such that the electron group velocity v does (not) change its sign: $v \to v$ ($v \to -v$). When the group velocity of the photo-excited electron, which is given by $\partial E/\partial k$, has the same sign for the two electronic energy dispersions for the initial and the scattered states, then forward scattering occurs. Otherwise, backward scattering occurs.

[7] A conduction electron can be scattered by a phonon with wave-vector $q = 2k_{\rm F}$ from an occupied state below the Fermi energy $E_{\rm F}$ to an unoccupied state above $E_{\rm F}$ while conserving the Pauli principle and energy momentum.

Table 1: Properties of the various Raman features in graphite and SWNTs.[1)]

Name[2)]	ω[cm^{-1}]	Res.[3)]	$d\omega/dE_{\rm L}^{4)}$	Notes[5)]
iTA	288	DR1	129	iTA mode, AV-b
LA	453	DR1	216	LA mode, AV-b
RBM	$227/d_t$	SR	0	Nanotube only, vibration of radius
oTO	860	DR1	0	IR-active mode in graphite
D	1350	DR1	53	LO or iTO mode, AV-b
LO	1450	DR1	0	LO mode, EV-f
$G(M)$	1550	SR	0	G mode only for metallic carbons[6)]
G	1582	SR	0	Raman active mode of graphite[7)]
M^-	1732	DR2	–26	overtone of oTO mode, AV-b
M^+	1755	DR2	0	overtone of oTO mode, AV-f
iTOLA	1950	DR2	230	combinational mode of iTO and LA
G′	2700	DR2	106	overtone of D mode
2LO	2900	DR2	0	overtone of LO mode
2G	3180	DR2	0	overtone of G mode

[1)] Mode frequencies for dispersive modes are given at $E_{\rm laser} = 2.41$ eV.
[2)] For some modes, see reference (Dresselhaus *et al.*, 2005) for an explanation of the mode name.
[3)] The following notation is used to classify the Raman scattering process:
SR: 1st order; DR1: 1 phonon double resonance, DR2; 2 phonons, double resonance.
[4)] $d\omega/dE_{\rm L}$ denotes the change of the phonon frequency in cm^{-1} produced by changing the laser energy by 1 eV.
[5)] Double resonance (DR) features are classified as intra-valley (AV, K $\rightarrow$ K, $q \sim 0$) and inter-valley (EV, K $\rightarrow$ K′, $q \sim \Gamma\vec{K}$). and as forward (f) and backward (b) scattering.
[6)] This phonon mode was originally discussed by the Breit–Wigner–Fano lineshape, but now many groups have pointed out a softened G-band by the Kohn-anomaly (see Sec. 4.4).
[7)] G-band for graphite is at 1582 cm^{-1} (Piscanec *et al.*, 2004, Ando, 2006a). For SWNTs, there is a G^+ mode at 1590 cm^{-1} due to in-plane vibrations along the tube axis, and a diameter dependent G^- mode (at 1570 cm^{-1} for tubes with a diameter of 1.4nm) for in-plane vibrations along the circumferential direction (see §6.2.1).

softened by the Kohn anomaly effect. All phonon modes which have a strong Raman intensity (electron-phonon coupling) can be candidates for the Kohn anomaly. An additional requirement for the Kohn anomaly is that the vibrational displacement of the phonon is relevant to the opening of an energy gap at $E_{\rm F}$ (the Peierls instability)[8]. Among the various phonon modes, the LO phonon mode shows this Kohn anomaly for carbon nanotubes and graphene at the Γ and K (K′) points.

In the case of SWNTs generally, the G modes are split into G^+ (LO) and G^- (TO) modes. In the case of metallic SWNTs, the LO phonon mode becomes softer than the TO phonon mode and reaches a frequency ω_{G-} around $1550\,\mathrm{cm}^{-1}$. It is not yet established well enough to say that a G^+ phonon mode can be seen around $1590\,\mathrm{cm}^{-1}$ and that no TO phonon mode can be seen around $1570\,\mathrm{cm}^{-1}$ in the Raman spectrum for metallic SWNTs. Thus we expect that the TO and LO phonon modes exchange frequencies with each other for metallic tubes. Recent experiments on a graphene sheet using electro-chemical doping or electronic doping by a gate electrode show that the TO and LO phonon modes cross (or anti-cross) each other as a function of the variation of $E_{\rm F}$. (Pisana *et al.*, 2007) Another important experimental result concerns the Raman signals from graphite intercalation compounds in which only one softened G band spectra feature can be seen for different doping levels (Song *et al.*, 1976, Eklund *et al.*, 1977). Since a SWNT has Raman-active modes with A, E_1 and E_2 symmetry (Saito *et al.*, 1998b, Jorio *et al.*, 2000, 2003b), it would be important to consider the Kohn anomaly for all phonon modes for understanding the precise behavior of the G-band phonon modes.

4.5 Elastic scattering and the D-band

The photo-excited electron can be scattered elastically (measurements show that the energy is not changed in the scattering process) by defects, such as point defect and the edge of the crystal (boundary scattering) (Sato *et al.*, 2006, Cancado *et al.*, 2004, Pimenta *et al.*, 2007). An elastic scattering process can thus be substituted for one of the two scattering events in a second-order Raman process (see Fig. 4). In this case, only one phonon frequency with $q \neq 0$ participates in the scattering event. If one of the two scattering events of the G′ band process is an elastic scattering event, we instead see the double resonance Raman band at around $1350\,\mathrm{cm}^{-1}$ for 2.41 eV laser energy, and we call this phonon which is associated with a defect the D-band (disorder-induced feature). The D-band Raman intensity is strong when the number of defects in the sample is large or the sample size of the crystal is small and boundary scattering becomes important.

Since the G and G′ bands are intrinsic Raman signals that we can see even when there are no defects, the intensity ratio of the D-band related to the G-band (I_D/I_G) is frequently used to characterize a sample in terms of the defect density or the crystalline size.(Pimenta *et al.*, 2007)

Rayleigh scattering of light, which is known as the reason why the sky is blue, is the elastic scattering of light. When we see the optical process of Rayleigh scattering in a solid, the scattering of a photo-excited electron does not change in energy for the scattering event. The Rayleigh scattering is in one sense an annoying signal for Raman measurements since a

[8]When an energy gap is opened by a lattice vibration, a lattice distortion might result in a giant Kohn anomaly. This implies a strong electron-phonon coupling.

strong tail of the spectra line at $0\,\mathrm{cm}^{-1}$ interferes with the observation of the inelastic Raman signals. Thus we usually cut out the elastically scattered light by using laser-specific filters (notch filters). Similar to resonance Raman spectroscopy, the Rayleigh intensity is enhanced for the resonance condition for optical transitions (see for example, Chapter by T. F. Heinz in (Jorio *et al.*, 2007)). The resonance Rayleigh scattering technique is now also being used for determining the E_{ii} value for specific (n, m) SWNTs (Wang *et al.*, 2006).

4.6 Sample evaluation by Raman spectroscopy and photoluminescence

Here we list the way that a sample is characterized using Raman spectroscopy. If we want to know whether or not the sample contains SWNTs, we can check for the existence of an RBM signal. For given E_{laser}, the RBM signal would tell us that a resonance with a particular (n, m) SWNT exists. When the diameter range for SWNTs in the sample does not match the resonance condition, we can not see any signal. By checking the typical diameter distribution in a sample by TEM or by SPM, we can determine which E_{laser} is suitable for observing RBM spectra for a given sample. A sample synthesized by chemical vapor deposition (CVD) usually has a large diameter distribution from 0.8-2 nm, and we can easily find the RBM signal. If we can wrap a SWNT by some surfactant[9] such as SDS (sodium dodecyl sulfate) or DNA, we will see the distribution of SWNTs in the photoluminescence (PL) spectra for the semiconducting SWNTs in the sample. In PL spectroscopy, we can change the excitation energy easily if we use a lamp with a continuous range of wavelengths. The photo-absorption occurs at E_{22} for a conventional range of photon wavelengths, and the photo-excited carriers are relaxed quickly by emitting phonons to reach E_{11} and PL is then observed at E_{11}. When we now make a 2D map of the PL intensity as a function of the energies of photo-absorption and PL, many peaks appear, each peak corresponding to (n, m) for that tube (Jorio *et al.*, 2004, Bachilo *et al.*, 2002) (Fig. 6). Thus as far as we have a sample for which the SWNTs are suspended in water through a surfactant or wrapping agent, PL measurements are convenient and providing a powerful tool for determining the distribution of (n, m) semiconducting SWNTs in the sample. Raman measurements, on the other hand, have the merit that (1) we can measure a sample as it is prepared (no surfactant treatment is needed), and that (2) we can measure not only semiconductor SWNTs but also metallic SWNTs. In the case of metallic SWNTs, we do not see the PL spectra, since the photo-excited carriers non-radiatively decay into the metallic energy band at a speed ($\ll 1$ ps) that is much faster than the optical transition (1 ns). Thus in a SWNT bundle, we expect a rapid energy transfer from a semiconducting SWNT to a metallic SWNT, and no SWNTs remain in an excited state long enough for PL emission to be observed (Jiang *et al.*, 2005c). Thus individual SWNTs that are isolated from other SWNTs by a surfactant or suspended between two electrodes in the air are needed to observe PL.

The (n, m) assignment is generally done by measuring the RBM frequency which is used in comparing with the prediction coming from the Kataura plot. The metallicity (metal or semiconductor) of a SWNT can usually be determined by the G band spectra. In the case of the G band, the G^- feature for a metallic SWNT can go down to as low as $1550\,\mathrm{cm}^{-1}$ (see Sec. 4.4) and the spectra becomes broad. For a conventional laser energy (from 1.5-2.5 eV), the G′ band

[9] There are many known surfactants that can be used for suspending SWNTs in water.

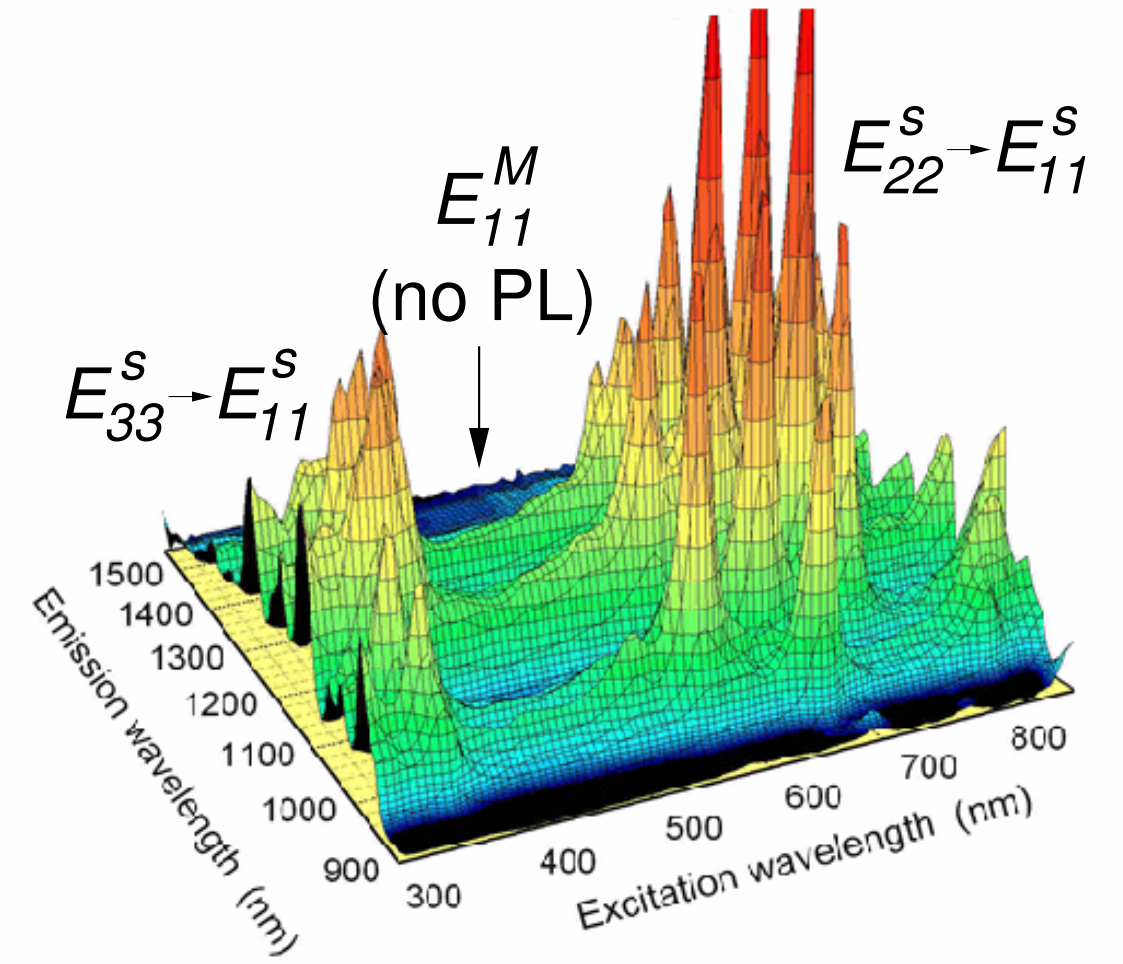

Figure 6: Photoluminescence spectra of isolated single wall carbon nanotubes as a function of emission wavelength and excitation wavelength. Each peak corresponds to a (n, m) semiconductor SWNT. For E_{11}^{M} energies, we do not have a PL peak.(Jorio *et al.*, 2004, Bachilo *et al.*, 2002)

intensity relative to the G band intensity is strong for metallic SWNTs or graphene. The chiral angle of a SWNT can be estimated in two ways: (1) the RBM signal is generally strong for zigzag nanotubes[10], (2) the G^- band intensity relative to the G^+ band intensity becomes strong for armchair nanotubes. These behaviors come from the diameter and chirality dependence of the electron-phonon coupling matrix element for the each phonon modes.(Jorio *et al.*, 2005a, Jiang *et al.*, 2007b, 2005a) For an isolated single nanotube laid on a TEM grid, we can directly determine its (n, m) values by the electron diffraction method, which can be used for SWNTs with d_t up to 3 nm. (Paillet *et al.*, 2006)

In addition to the RBM frequency, the RBM intensity also provides information regard-

[10]The PL intensity is strong for large chiral angles close to armchair nanotubes and for Type I relative to Type II semiconductor SWNTs. (Bachilo *et al.*, 2002)

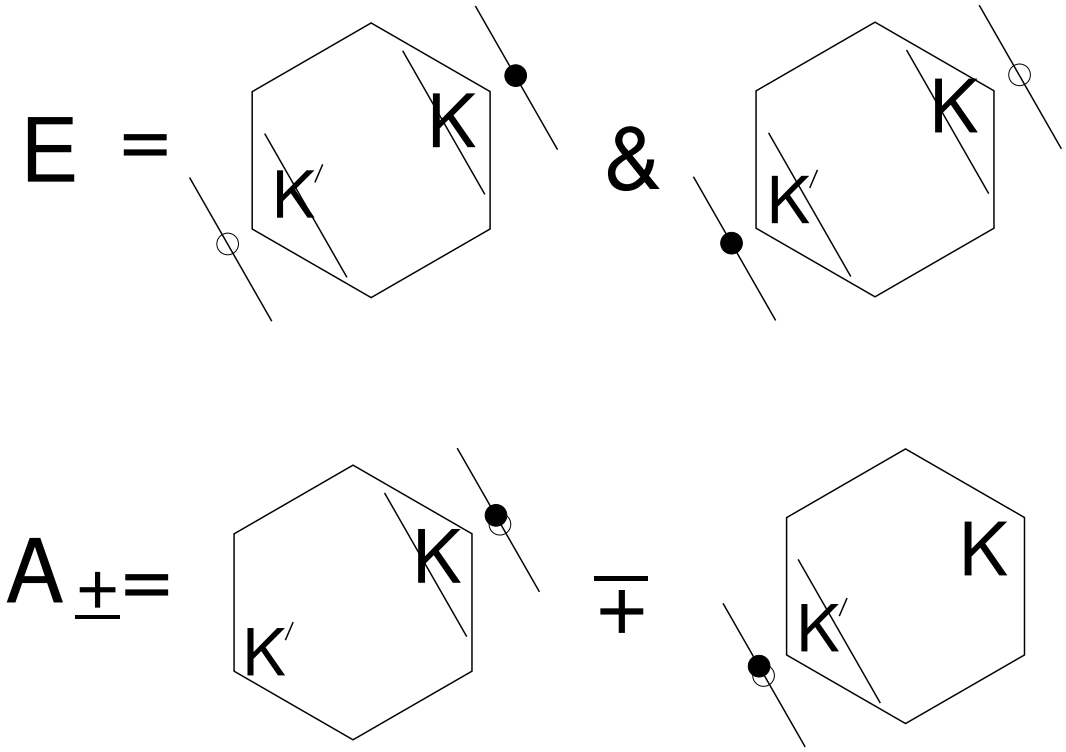

Figure 7: (a) E and (b) A symmetry excitons in SWNTs. Solid (open) circles denote an electron (a hole).

ing the (n, m) assignment and population estimation. Due to the unique exciton-phonon and exciton-photon matrix elements in SWNTs, the RBM intensity shows regular $(2n + m)$ family patterns, i.e., (1) the intensity has a large value near zigzag tubes while it has a small value near armchair tubes, (2) the intensity has a larger value for a VHS along KM than that along $K\Gamma$, (3) the intensity has a strong diameter dependence due to the exciton-photon matrix elements. (Jiang *et al.*, 2005b,a, Jorio *et al.*, 2005b, Popov *et al.*, 2005, Jiang *et al.*, 2007b)

5 EXCITONS IN SINGLE WALL CARBON NANOTUBES

5.1 Dark and Bright excitons

As we discussed in the overview section, the exciton of a SWNT is always formed upon photo excitation even at the room temperature. (Wang *et al.*, 2005, Chou *et al.*, 2005, Maultzsch *et al.*, 2005) Although the story for excitons for SWNTs is complicated, we try to offer here a basic explanation that is as simple as possible[11]. An exciton is a bound pair of a photo-excited electron (e) and a hole (h). For a photo-excited e-h pair, we expect the wave-vector of the electron and the hole to appear at the same position around the K or K′ point. However, since we expect

[11] We will consider here only the case of light polarized parallel to the nanotube axis. For a detailed discussion of the symmetry of the exciton, see references (Dresselhaus *et al.*, 2007, Jiang *et al.*, 2007b,a)

the scattering of the electron (or the hole) by the phonon, the electron and the hole can have different k vectors. Since we have two regions for possible k vectors around points K and K′, we have four possibilities of the positions of the electron and the hole for an exciton, such as (K, K), (K, K′), (K′, K) and (K′, K′) (see Fig. 7). The excitonic states for (K, K′) and (K′, K) are energetically degenerate, and we call them E symmetry excitons because they transform into one another by time inversion symmetry. Since the position of the electron and hole are different from each other for the E exciton, the E exciton can not be recombined to emit a photon, even though such an e-h pair feels an attractive Coulomb interaction in real space. Thus the E exciton is a dark exciton. As for the (K, K) and (K′, K′) e-h pairs, the two states have the same energy and are therefore strongly mixed with each other to make symmetry-adopted non-degenerate exciton states, such as (K, K) $\pm$ (K′, K′), which we denote by the $A\mp$ excitons[12]. The symmetry operation is a C_2 rotational symmetry operation around the axis perpendicular to the nanotube axis, which turns the SWNT upside down. Since the exciton wave-function for $A-$ ($A+$) is odd (even) under this symmetry operation and since the electron-photon Hamiltonian is odd, only the $A-$ exciton is optically allowed ($\langle$ exciton (odd) | Hamiltonian (odd) | ground state (even)$\rangle \neq 0$). An important point is that the even symmetry $A+$ exciton has a lower energy than the $A-$ exciton. Thus even though the $A-$ exciton is formed by light, the $A-$ exciton easily decays to the $A+$ exciton to reach the thermal equilibrium distribution. This is the main reason why the quantum efficiency of a SWNT is so low (several percent at most). The energy gap between the lowest energy exciton $A+$ and the bright exciton $A-$ is of the order of 1-10 meV and thus the PL intensity has a temperature dependence around 10-100 K.

5.2 GW correction and Bethe–Salpeter Equation

The coupled electron-hole excitation energies Ω and wave functions Ψ can be obtained by solving the Bethe–Salpeter equation (BSE), (Spataru *et al.*, 2004, Jiang *et al.*, 2007a, Perebeinos *et al.*, 2004, Dresselhaus *et al.*, 2007, Ando, 2006b)

$$\left\{[E(\boldsymbol{k}_{\rm c}) - E(\boldsymbol{k}_{\rm v})] + K(\boldsymbol{k}_{\rm c}^{'}\boldsymbol{k}_{\rm v}^{'}, \boldsymbol{k}_{\rm c}\boldsymbol{k}_{\rm v})\right\} \Psi^n(\boldsymbol{k}_{\rm c}\boldsymbol{k}_{\rm v}) = \Omega_n \Psi^n(\boldsymbol{k}_{\rm c}^{'}\boldsymbol{k}_{\rm v}^{'}), \tag{8}$$

where $\boldsymbol{k}_{\rm c}$ and $\boldsymbol{k}_{\rm v}$ denote wave-vectors of the conduction and valence energy bands and $E(\boldsymbol{k}_{\rm c})$ and $E(\boldsymbol{k}_{\rm v})$ are the quasi-electron and quasi-hole energies, respectively. $K(\boldsymbol{k}_{\rm c}^{'}\boldsymbol{k}_{\rm v}^{'}, \boldsymbol{k}_{\rm c}\boldsymbol{k}_{\rm v})$ is the electron-hole interaction kernel.

The Coulomb effect appears not only for e-h pairs but also for photo-excited electron (hole) and many valence electrons. The latter interaction increases the energy of the electron (decreases the energy of a hole), and this interaction thus contributes to the increase in the energy gap compared with the single-particle energy difference between an electron and a hole. This energy difference is called the self-energy. The self-energy is calculated by the GW approximation (Ando, 2006b, Spataru *et al.*, 2004, Jiang *et al.*, 2007a, Dresselhaus *et al.*, 2007), where the self-energy is a convolution of the non-interacting Green functions G and the screened Coulomb interaction W. (Aulbur *et al.*, 2000, Aryasetiawan and Gunnarsson, 1998) The corresponding Feynman diagram is shown in Fig. 8(a). Because of electron-electron interaction, the

[12]The notation of $A+$ is used for a bright exciton by some other groups. In any case, the bright exciton has an odd symmetry under C_2 rotation (Jiang *et al.* (2007a)).

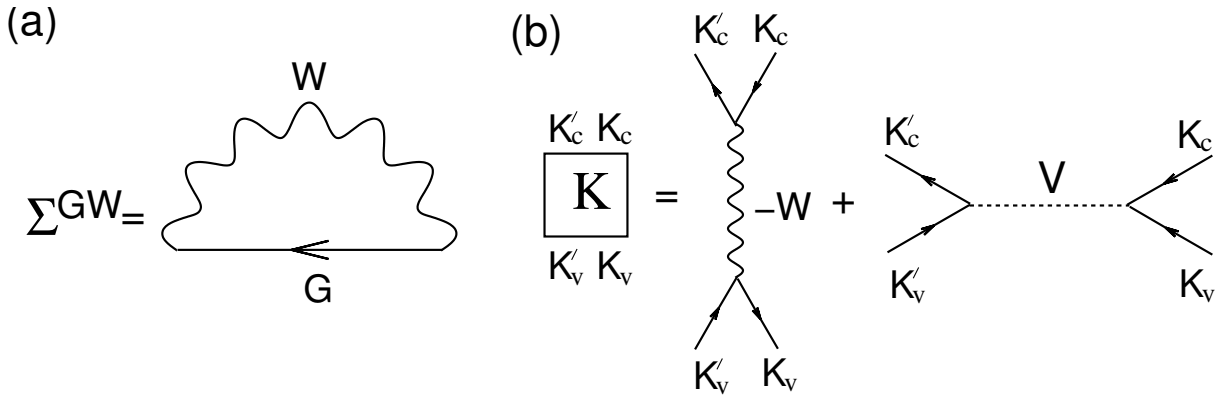

Figure 8: Feynman diagrams for the (a) GW approximation for the self-energy Σ and the (b) electron-hole interaction Kernel in the BSE's. In (b) wiggle and dashed lines represent screened and bare Coulomb interactions, respectively.

wave-vector k in the lattice is no longer a good quantum number and has a life time. Thus the electron (hole) is treated as a quasi-particle within its life time and an energy uncertainty for the quasi-particle energy occurs.

The kernel K in Eq. (8) has direct and exchange terms. (Spataru *et al.*, 2004, Jiang *et al.*, 2007a, Onida *et al.*, 2002). Fig. 8(b) shows the Feynman diagram for the kernel. The exchange term determines the energy splitting between the spin-singlet and triplet states. The exciton excitation energy is thus given by (single-particle energy) + (self energy) - (exciton binding energy) $\equiv$ (quasi-particle energy) - (exciton binding energy). We call (self energy) - (exciton binding energy) the many body effect. In SWNTs both the self-energy and exciton binding energy show $(2n + m)$ family patterns (see Fig. 9) (Jiang *et al.*, 2007a, Dresselhaus *et al.*, 2007). The many-body correction to E_{11} and E_{22} energies is around $0.2\,\mathrm{eV}$ while the correction to E_{33} and E_{44} energies can be $0.6\,\mathrm{eV}$ (Jiang *et al.*, 2007a, Dresselhaus *et al.*, 2007, Sato *et al.*, 2007a). Moreover, the many-body correction does not contribute to the family spread in E_{11} and E_{22} in the Kataura plot while it contributes significantly to the family spread in E_{33} and E_{44}. (Jiang *et al.*, 2007a, Dresselhaus *et al.*, 2007, Sato *et al.*, 2007a)

5.3 Localization of the wave-function

The delocalized Block functions with different k are mixed with one another. Since the exciton wave-function has a Gaussian shape along the nanotube axis direction, the mixing coefficient for k shows a Gaussian distribution whose center is a van Hove singular k point. (Jiang *et al.*, 2007b) Since the size of the exciton wave-function is larger than the diameter d_t of a SWNT (around 1-10 nm depending on d_t), (Dresselhaus *et al.*, 2007, Spataru *et al.*, 2004) the mixing coefficient has a large value for only one cutting line of the 1D Brillouin zone and thus the wave-function is almost constant around the circumferential direction of a nanotube.

Because of the localization of the exciton wave-function, optical transition matrix elements for an exciton are enhanced by one order of magnitude relative to the matrix element for a free e-h pair. (Jiang *et al.*, 2007b) This enhancement facilitates the observation of single SWNT

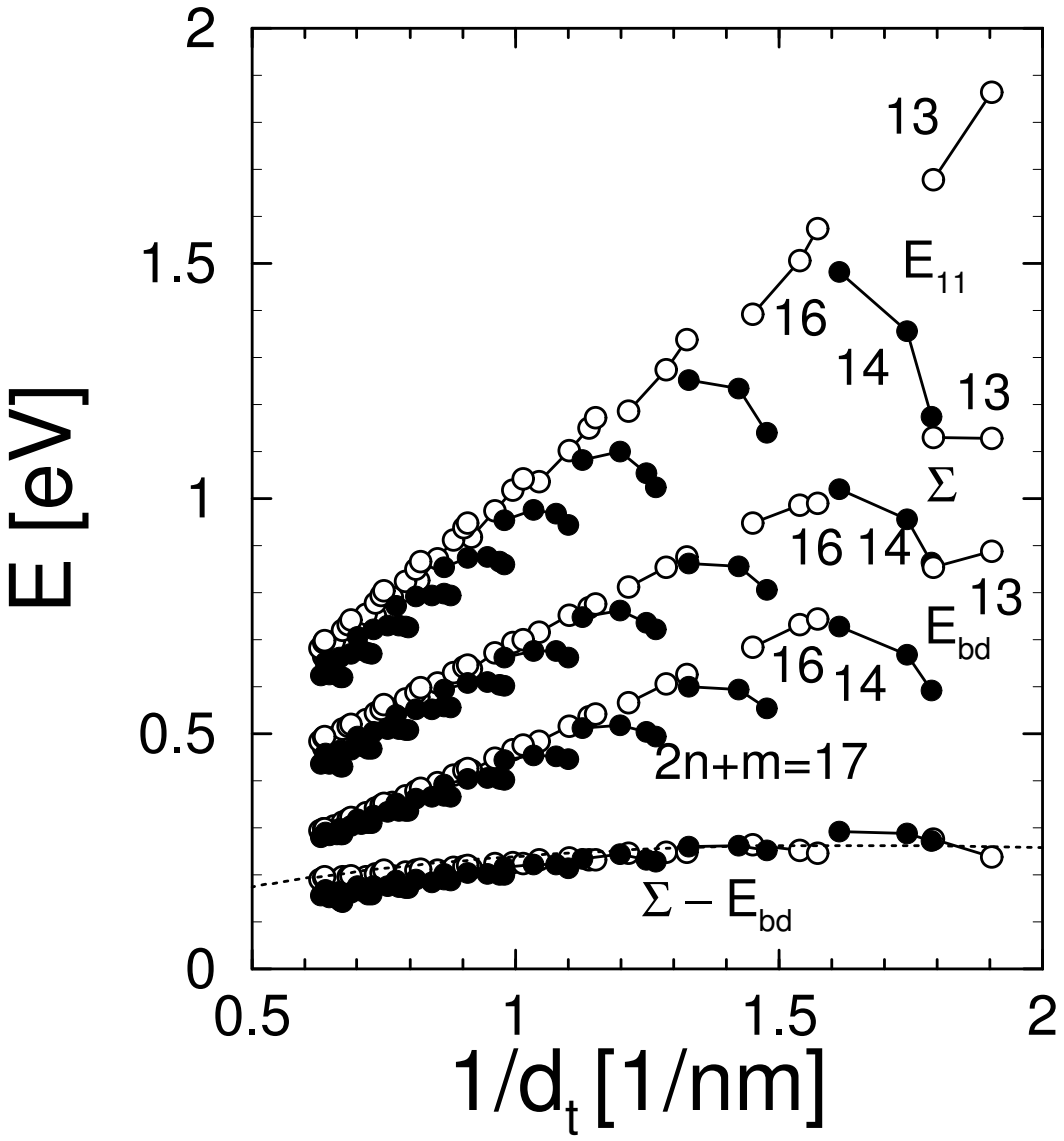

Figure 9: The excitation energy E_{11}, self-energy Σ, binding energy $E_{\rm bd}$ and energy corrections $\Sigma - E_{\rm bd}$ based on the extended tight binding method for E_{11} bright exciton states. Open and filled circles are for SI and SII SWNTs. The dashed line is calculated by $E^{\log} = 0.55(2p/3d_t)\log[3/(2p/3d_t)]$ with $p = 1$(Jiang *et al.*, 2007a,b).

spectroscopy by Raman and PL spectroscopy.

5.4 Spin of the exciton

When we consider an exciton, there is an additional freedom for the exciton states associated with the spin. (Dresselhaus *et al.*, 2007) We have a spin-singlet (S=0) and three spin-triplet (S=1) exciton states for each of the four symmetry exciton states. Thus the exciton states have 16 possible states for a given E_{ii}. Since the singlet exciton is generated by an optical transition, the spin-triplet exciton is a dark exciton. However, when we consider a spin flipping mechanism such as a magnetic field, the triplet exciton can be coupled with the singlet exciton and made bright. This can be demonstrated by the spectra change in the PL spectra in the presence of a magnetic field (Ando, 2006b, Zaric *et al.*, 2006). The triplet states are somewhat (1-100 meV) below the singlet states and thus they also contribute to the low PL quantum efficiency of a SWNT (Spataru *et al.*, 2005).

5.5 Exciton phenomena in the Raman and PL spectra

Recent Raman and PL experiments show that exciton properties are essential for understanding these photo-physical observations. Here we list the important phenomena related to these excitons.

For RBM and G band Raman intensities, the chirality dependence which are mainly determined by exciton-phonon matrix elements, are not sensitive to the exciton effects. However, exciton effects enhance the magnitude and diameter dependence of the Raman intensities through the exciton-photon matrix elements. (Jiang *et al.*, 2007b).

The E_{ii} values can be modified by contact with environmental materials, which we call environmental effects. (Miyauchi *et al.*, 2007) Whatever energy upshifts or downshifts are observed depend on whether the semiconductor SWNTs is type I and type II, and the value of i in E_{ii}, and the SWNT diameter. The magnitude of the shift in energy depends on the dielectric constant of the environmental material. This situation is similar to the behavior of the exciton energy for the hydrogen atom, which depends on the dielectric constant by substituting e^2/ϵ for e^2 in $me^4/2\hbar^2$ in the hydrogen 1s orbital. The part of the electric field between the e-h pair of the exciton that lies outside of the SWNT will affect the exciton energy. Since the electric field also penetrates into the nanotube itself, the dielectric response of the π electron is important, too. An important point is that even a metallic SWNT has an exciton binding energy, though it is relatively small in comparison to that of semiconducting SWNTs. The environmental effect is proportional to the many body effect values which is scaled by the reduced mass of the e-h pair and the dielectric constant of the surrounding materials. Since the effective mass of the electron and hole depend significantly on the type (type I or II) of the semiconductor nanotube, which is understood by the trigonal warping effect, the many body effect depends on the type of the semiconducting SWNTs.

Another example of an experiment that is sensitive to the excitonic nature of the photophysical processes is the two-photon absorption experiment. (Wang *et al.*, 2005) Since the two-photon absorption has a different allowed symmetry for the initial and final states, the mea-

surements can probe the first excited exciton states (even symmetry) directly. This measurement was able to clearly distinguish between the exciton story and band-to-band excitation absorption and emission, to make it clear that excitonic processes dominate the photophysics of nanotubes.

Scanning transmission spectroscopy and transport experiments are related to one-particle excitation, where the carriers have a self-energy but no exciton binding energy. Thus the observed energy gap from such measurements give a clear distinction between the single (quasi) particle picture and the exciton-bound electron.

6 SUMMARY AND FUTURE DIRECTIONS

In summary, we have discussed here the unique electronic structure of graphene and SWNTs. One dimensional materials are expected to have a singular joint density of electronic states which gives rise to a sharp spectral feature associated with transition energies E_{ii} appearing in resonance Raman and PL spectra. From the RBM spectra and by using the Kataura plot, we can determine the nanotube diameter and (n, m) values for a resonant SWNT. The double-cone structure of the energy dispersion at the Fermi energy around the K and K′ point is responsible for many exotic phenomena observed in the Raman spectra, not only for the intra-valley scattering but also for the inter-valley scattering phonon modes. The existence of a Fermi surface in doped graphene and metallic SWNTs is also relevant to the Kohn anomaly for the G-band phonon mode. The inter-valley scattering effect for the $q \neq 0$ phonon modes can be seen in the second-order Raman scattering for which a double resonance condition for the Raman spectra provides as strong a signal as that of the first-order of Raman spectra. Because of the linear energy dispersion of the electronic structure of SWNTs and graphene, a dispersive $\partial\omega/\partial E_{\rm laser}$ behavior can be seen in the second-order overtone and combinational phonon mode frequencies. When one of the two scattering processes in the second-order Raman spectra is an elastic scattering event induced by defects or the boundary of the crystal, defect-induced Raman features, such as the D-band can be seen, which is useful for evaluating the defect density or the crystallite size from measurement of the I_D/I_G intensity ratio. Excitons are essential for describing optically excited e-h pairs and the existence of not only bright excitons but also dark excitons have already been demonstrated by many high magnetic field and low temperature experimental results (Zaric *et al.*, 2004, 2006). The localization of the exciton wave-function contributes significantly to the enhancement of optical transitions in nanotubes (Jiang *et al.*, 2007b).

Since Raman spectroscopy clearly reveals many aspects of nanotube physics, it is now possible to go into great detail about the photophysics of nanotubes in the frequency domain. On the other hand, many open issues remain to be addressed about the dynamics of photo-excited carriers (Hiroki *et al.*, 2006) which are expected to be more intensively investigated in future work. When the laser pulse is sufficiently short compared to the time of a single vibration, we can see coherent phonons (RBM, and even G-band vibrations in the case of SWNTs) excited by the light through the electron-phonon interaction (Lim *et al.*, 2006). Transmission spectroscopy studies of such coherent phonons are now providing another spectroscopic technique to observe specific phonons. When the light pulse is sufficiently strong, the optical absorption is saturated and the material becomes transparent. Saturated optical absorption provides an interesting technique for studying non-linear optical phenomena. This approach is also important for possible

applications in a mode-locked laser for a fast optical switch (on the order of 10 fs) by using SWNTs as a saturated absorber especially designed for 1.54 μm operation at the telecommunication wavelength of optical fibers (Rozhin *et al.*, 2006) .

One weak point about confocal micro-Raman spectroscopy is its relatively poor spatial resolution of around 1 μm, which is not sufficient for nano-technology applications. Using a non-propagating light beam at the tiny (10 nm) aperture of the tip of an optical fiber, a much smaller spatial resolution can be achieved in a Raman spectroscopy related experiment. This approach has matured in the past few years and is called near field optics (near field Raman and PL, see for example, Chapter by Y-Z. Ma et al. in (Jorio *et al.*, 2007)). It is expected that near field optics will become an important technique for the next generation of photophysics. Carrier injection and exciton formation are important for semiconductor-SWNT photo devices and for this reason exciton dynamics in SWNTs will also become an interesting subject. Bi-exciton formation in a SWNT is a new topic at an early stage of investigation, while an Auger process has been identified as an important process for dissociating two excitons (Chapter by Y-Z. Ma et al. in (Jorio *et al.*, 2007)).

Nanometer devices made with a graphene ribbon are now becoming popular. Because of the singular behavior of the quantum Hall effect in graphene, many unusual transport properties have been observed (Geim and Novoselov, 2007). Excitonic effects should be observed in a narrow graphene ribbon in analogy to the many excitonic effects that have been seen in SWNTs. The exciton physics of a metallic SWNT is an especially interesting subject in which the dynamic, dielectric response of the exciton will be a key issue for gaining further understanding of environmental effects in metallic SWNTs.

A new nano-structure of a linear single atom carbon chain structure encapsulated in the core of a SWNT is an ultimate 1D carbon material (Zhao *et al.*, 2003, Nishide *et al.*, 2006, 2007). The study of the photophysics of the nano-chain of carbon would be a very interesting fundamental subject for future study. From the standpoint of metrology, measurements of the absolute value of the Raman intensity will be important as a standard for evaluating the signal from a nanotube (or graphene) sample observed under many different conditions (See, for example, Chapter by A. Jorio et al. in (Jorio *et al.*, 2007)). The fabrication of photo-devices based on SWNTs on Si or other semiconductors will become more important in the future. In this case, the energy transfer of photo-excited carriers between two SWNTs whose length and distance is of the order of the wavelength of light will become an important subject not only for nano-science but also for nano-technology.

Experimental techniques for nano-science and technology should be improved, making use of the many possibilities introduced by carbon nanotubes and other new materials now available at the nano-scale. For example, in resonance Raman spectroscopy, a quick and continuous change of $E_{\rm laser}$ without changing the focused position in the sample is highly desired. The technique for making fiducial marks on a sample and combining spectroscopy with TEM and SPM will become increasingly important. Thus there are many opportunities in nano-science and nano-technology for both SWNTs and graphene to continue to have a large impact on other fields of science and on other areas of technology.

The authors thank their many collaborators and coworkers for many discussion and comments. R.S. acknowledges a Grant-in-Aid (No. 16076201) from the Ministry of Education,

Japan. A.J. acknowledges financial support by PRPq-UFMG, FAPEMIG and CNPq, Brazil. MIT authors acknowledge support under NSF Grant DMR 04-05538.

References

Ando, T. (1997), *J. Phys. Soc. Jpn.*, **66**, 1066.

Ando, T. (2006a), *J. Phys. Soc. Jpn.*, **75**, 124701.

Ando, T. (2006b), *J. Phys. Soc. Jpn.*, **75**, 024707.

Araujo, P. T., Doorn, S. K., Maruyama, S., Chacham, H., Pimenta, M. A., and Jorio, A. (2007), *Phys. Rev. Lett.*, **98**, 1012.

Aryasetiawan, F. and Gunnarsson, O. (1998), *Rep. Prog. Phys.*, **61**, 237.

Aulbur, W. G., Jönsson, L., and Wilkins, J. W. (2000), *Solid State Physics*, **54**, 1.

Bachilo, S. M., Strano, M. S., Kittrell, C., Hauge, R. H., Smalley, R. E., and Weisman, R. B. (2002), *Science*, **298**, 2361.

Barros, E. B., Jorio, A., Samsonidze, G. G., Capaz, R. B., Filho, A. G. S., Filho, J. M., Dresselhaus, G., and Dresselhaus, M. S. (2006a), *Physics Reports*, **431**, 261.

Barros, E. B., Capaz, R. B., Jorio, A., Samsonidze, G. G., Filho, A. G. S., Ismail-Beigi, S., Spataru, C. D., Louie, S. G., Dresselhaus, G., and Dresselhaus, M. S. (2006b), *Phys. Rev. B Rapid*, **73**, 241406(R).

Cancado, L. G., Pimenta, M. A., B. R. A. Neves, M. S. S. D., and Jorio, A. (2004), *Phys. Rev. Lett.*, **93**, 247401.

Cancado, L. G., Takai, K., Enoki, T., Endo, M., Kim, Y. A., Mizusaki, H., Jorio, A., Coelho, L. N., Magalhaes-Paniago, R., and Pimenta, M. A. (2006), *Appl. Phys. Lett.*, **88**, 163106.

Cardona, M. (1982). *Light Scattering in Solids II: edited by M. Cardona and G. Güntherodt*, volume 50, pages 19. Springer-Verlag, Berlin. Chapter 2, Topics in Applied Physics.

Chou, S. G., Plentz Filho, F., Jiang, J., Saito, R., Nezich, D., Ribeiro, H. B., Jorio, A., Pimenta, M. A., Samsonidze, G. G., Santos, A. P., Zheng, M., Onoa, G. B., Semke, E. D., Dresselhaus, G., and Dresselhaus, M. S. (2005), *Phys. Rev. Lett.*, **94**, 127402.

Doorn, S. K., Heller, D. A., Barone, P. W., Usrey, M. L., and Strano, M. S. (2003), *Appl. Phys. A*, **78**, 1147.

Doorn, S. K., Heller, D. A., Barone, P. W., Usrey, M. L., and Strano, M. S. (2004), *Appl. Phys. A*, **78**, 1147.

Dresselhaus, M. S., Dresselhaus, G., Saito, R., and Jorio, A. (2005), *Physics Reports*, **409**, 47.

Dresselhaus, M. S., Dresselhaus, G., Saito, R., and Jorio, A. (2007). In S. R. Leone, J. T. Groves, R. F. Ismagilov, and G. Richmond, editors, *Annual Reviews of Physical Chemistry Chemical Physics*, volume 58, pages 719, Palo Alto, CA. Annual Reviews.

Duesberg, G. S., Loa, I., Burghard, M., Syassen, K., and Roth, S. (2000), *Phys. Rev. Lett.*, **85**, 5436.

Eklund, P. C., Dresselhaus, G., Dresselhaus, M. S., and Fischer, J. E. (1977), *Phys. Rev. B*, **16**, 3330.

Fantini, C., Jorio, A., Souza, M., Strano, M. S., Dresselhaus, M. S., and Pimenta, M. A. (2004), *Phys. Rev. Lett.*, **93**, 147406.

Geim, A. K. and Novoselov, K. S. (2007), *Nature Mater.*, **6**, 183.

Hamada, N., Sawada, S., and Oshiyama, A. (1992), *Phys. Rev. Lett.*, **68**, 1579.
Hartschuh, A., Pedrosa, H. N., Novotny, L., and Krauss, T. D. (2003), *Science*, **301**, 1354.
Hiroki, H., Matsuda, K., Miyauchi, Y., Maruyama, S., and Kanemitsu, Y. (2006), *Phys. Rev. Lett.*, **97**, 257401.
Iijima, S. (1991), *Nature (London)*, **354**, 56.
Jiang, J., Saito, R., Samsonidze, G. G., Chou, S. G., Jorio, A., Dresselhaus, G., and Dresselhaus, M. S. (2005a), *Phys. Rev. B*, **72**, 235408.
Jiang, J., Saito, R., Grüneis, A., Chou, S. G., Samsonidze, G. G., Jorio, A., Dresselhaus, G., and Dresselhaus, M. S. (2005b), *Phys. Rev. B*, **71**, 205420.
Jiang, J., Saito, R., Grüneis, A., Chou, S. G., Samsonidze, G. G., Jorio, A., Dresselhaus, G., and Dresselhaus, M. S. (2005c), *Phys. Rev. B*, **71**, 045417.
Jiang, J., Saito, R., Samsonidze, G. G., Jorio, A., Chou, S. G., Dresselhaus, G., and Dresselhaus, M. S. (2007a), *Phys. Rev. B*, **75**, 035407.
Jiang, J., Saito, R., Sato, K., Park, J. S., Samsonidze, G. G., Jorio, A., Dresselhaus, G., and Dresselhaus, M. S. (2007b), *Phys. Rev. B*, **75**, 035405.
Jorio, A., Dresselhaus, G., Dresselhaus, M. S., Souza, M., Dantas, M. S. S., Pimenta, M. A., Rao, A. M., Saito, R., Liu, C., and Cheng, H. M. (2000), *Phys. Rev. Lett.*, **85**, 2617.
Jorio, A., Saito, R., Hafner, J. H., Lieber, C. M., Hunter, M., McClure, T., Dresselhaus, G., and Dresselhaus, M. S. (2001), *Phys. Rev. Lett.*, **86**, 1118.
Jorio, A., Souza Filho, A. G., Dresselhaus, G., Dresselhaus, M. S., Swan, A. K., Ünlü, M. S., Goldberg, B., Pimenta, M. A., Hafner, J. H., Lieber, C. M., and Saito, R. (2002), *Phys. Rev. B*, **65**, 155412.
Jorio, A., Pimenta, M. A., Souza Filho, A. G., Saito, R., Dresselhaus, G., and Dresselhaus, M. S. (2003a), *New Journal of Physics*, **5**, 1.1.
Jorio, A., Pimenta, M. A., Souza Filho, A. G., Samsonidze, G. G., Swan, A. K., Ünlü, M. S., Goldberg, B. B., Saito, R., Dresselhaus, G., and Dresselhaus, M. S. (2003b), *Phys. Rev. Lett.*, **90**, 107403.
Jorio, A., Saito, R., Hertel, T., Weisman, R. B., Dresselhaus, G., and Dresselhaus, M. S. (2004), *Bulletin of the Materials Research Society*, **29**, 276.
Jorio, A., Santos, A. P., Ribeiro, H. B., Fantini, C., Souza, M., Vieira, J. P. M., Furtado, C. A., Jiang, J., Balzano, L., Resasco, D. E., and Pimenta, M. A. (2005a), *Phys. Rev. B*, **72**, 075207.
Jorio, A., Fantini, C., Pimenta, M. A., Capaz, R. B., Samsonidze, G. G., Dresselhaus, G., Dresselhaus, M. S., Jiang, J., Kobayashi, N., Grüneis, A., and Saito, R. (2005b), *Phys. Rev. B*, **71**, 075401.
Jorio, A., Dresselhaus, M. S., and Dresselhaus, G. (2007). *Carbon Nanotubes: Advanced Topics in the Synthesis, Structure, Properties and Applications*, volume 111 of *Springer Series in Topics in Appl. Phys.* Springer-Verlag, Berlin.
Lim, Y. S., Yee, K. J., Kim, J. H., Haroz, E. H., Shaver, J., Kono, J., Doorn, S. K., Hauge, R. H., and Smalley, R. E. (2006), *Nano Lett.*, **6**, 2696.
Mahan, G. D. (2002), *Phys. Rev. B*, **65**, 235402.
Martin, R. M. and Falicov, L. M. (1983). *Light Scattering in Solids I: edited by M. Cardona*, volume 8, pages 79. Springer-Verlag, Berlin. Chapter 3, Topics in Applied Physics.
Matthews, M. J., Pimenta, M. A., Dresselhaus, G., Dresselhaus, M. S., and Endo, M. (1999),

Phys. Rev. B, **59**, R6585.
Maultzsch, J., Pomraenke, R., Reich, S., Chang, E., Prezzi, D., Ruini, A., Molinari, E., Strano, M. S., Thomsen, C., and Lienau, C. (2005), *Phys. Rev. B*, **72**, 241402.
Miyauchi, Y., Saito, R., Sato, K., Ohno, Y., Iwasaki, S., Mizutani, T., Jiang, J., and Maruyama, S. (2007), *Chem. Phys. Lett.*, **442**, 394.
Nishide, D., Dohi, H., Wakabayashi, T., Nishibori, E., Aoyagi, S., Ishida, M., Kikuchi, S., Kitaura, R., Sugai, T., Sakata, M., and Shinohara, H. (2006), *Chem. Phys. Lett.*, **428**, 356.
Nishide, D., Wakabayashi, T., Sugai, T., Kitaura, R., Kataura, H., Achiba, Y., and Shinohara, H. (2007), *J. Phys. Chem. C*, **111**, 5178.
Novoselov, K. S., Geim, A. K., Morozov, S. V., Jiang, D., Katsnelson, M. I., Grigorieva, I. V., Dubonos, S. V., and Firsov, A. A. (2005), *Nature*, **438**, 197.
Onida, G., Reining, L., and Rubio, A. (2002), *Rev. Mod. Phys.*, **74**, 601.
Paillet, M., Michel, T., Meyer, J. C., Popov, V. N., Henrard, L., Roth, S., and Sauvajol, J.-L. (2006), *Phys. Rev. Lett.*, **96**, 257401.
Pedersen, T. G. (2003), *Phys. Rev. B*, **67**, 073401.
Perebeinos, V., Tersoff, J., and Avouris, P. (2004), *Phys. Rev. Lett.*, **92**, 257402.
Pfeiffer, R., Simon, F., Kuzmany, H., and Popov, V. N. (2005), *Phys. Rev. B*, **72**, 161404.
Pimenta, M. A., Dresselhaus, G., Dresselhaus, M. S., Cançado, L. G., Jorio, A., and Saito, R. (2007), *Physical Chemistry Chemical Physics*, **9**, 1276.
Pisana, S., Lazzeri, M., Casiraghi, C., Novoselov, K. S., Geim, A. K., Ferrari, A. C., and Mauri, F. (2007), *Nature Materials*, **6**, 198.
Piscanec, S., Lazzeri, M., Mauri, M., Ferrari, A. C., and Robertson, J. (2004), *Phys. Rev. Lett.*, **93**, 185503.
Piscanec, S., Lazzeri, M., Robertson, J., Ferrari, A. C., and Mauri, F. (2007), *Phys. rev. B*, **75**, 035427.
Popov, V. N., Henrard, L., and Lambin, P. (2005), *Phys. Rev. B*, **72**, 035436.
Rao, A. M., Richter, E., Bandow, S., Chase, B., Eklund, P. C., Williams, K. W., Fang, S., Subbaswamy, K. R., Menon, M., Thess, A., Smalley, R. E., Dresselhaus, G., and Dresselhaus, M. S. (1997), *Science*, **275**, 187.
Rozhin, A. G., Sakakibara, Y., Namiki, S., Tokumoto, M., Kataura, H., and Achiba, Y. (2006), *Appl. Phys. Lett.*, **88**, 051118.
Saito, R., Fujita, M., Dresselhaus, G., and Dresselhaus, M. S. (1992a), *Appl. Phys. Lett.*, **60**, 2204.
Saito, R., Fujita, M., Dresselhaus, G., and Dresselhaus, M. S. (1992b), *Phys. Rev. B*, **46**, 1804.
Saito, R., Dresselhaus, G., and Dresselhaus, M. S. (1998a). *Physical Properties of Carbon Nanotubes*. Imperial College Press, London.
Saito, R., Takeya, T., Kimura, T., Dresselhaus, G., and Dresselhaus, M. S. (1998b), *Phys. Rev. B*, **57**, 4145.
Saito, R., Jorio, A., Hafner, J. H., Lieber, C. M., Hunter, M., McClure, T., Dresselhaus, G., and Dresselhaus, M. S. (2001), *Phys. Rev. B*, **64**, 085312.
Saito, R., Jorio, A., Souza Filho, A. G., Dresselhaus, G., Dresselhaus, M. S., and Pimenta, M. A. (2002), *Phys. Rev. Lett.*, **88**, 027401.
Samsonidze, G. G., Saito, R., Jorio, A., Pimenta, M. A., Souza Filho, A. G., Grüneis, A., Dres-

selhaus, G., and Dresselhaus, M. S. (2003), *Journal of Nanoscience and Nanotechnology*, **3**, 431.
Samsonidze, G. G., Saito, R., Kobayashi, N., Grüneis, A., Jiang, J., Jorio, A., Chou, S. G., Dresselhaus, G., and Dresselhaus, M. S. (2004), *Appl. Phys. Lett.*, **85**, 5703.
Sato, K., Saito, R., Oyama, Y., Jiang, J., Cançado, L. G., Pimenta, M. A., Jorio, A., Samsonidze, G. G., Dresselhaus, G., and Dresselhaus, M. S. (2006), *Chem. Phys. Lett.*, **427**, 117.
Sato, K., Saito, R., Jiang, J., Dresselhaus, G., and Dresselhaus, M. S. (2007a), *Vibrational Spectroscopy*, **in press**. proofs 6/6/07: Fortaleza workshop: accepted.
Sato, K., Saito, R., Jiang, J., Dresselhaus, G., and Dresselhaus, M. S. (2007b), *Phys. Rev. B*.
Song, J. J., Chung, D. D. L., Eklund, P. C., and Dresselhaus, M. S. (1976), *Solid State Comm.*, **20**, 1111.
Spataru, C. D., Ismail-Beigi, S., Benedict, L. X., and Louie, S. G. (2004), *Phys. Rev. Lett.*, **92**, 077402.
Spataru, C. D., Ismail-Beigi, S., Capaz, R. B., and Louie, S. G. (2005), *Phys. Rev. Lett.*, **95**, 247402.
Strano, M. S. (2003), *J. Am. Chem. Soc.*, **125**, 16148.
Tanaka, K., Okada, M., Okahara, K., and Yamabe, T. (1992), *Chem. Phys. Lett.*, **191**, 469.
Telg, H., Maultzsch, J., Reich, S., Hennrich, F., and Thomsen, C. (2004), *Phys. Rev. Lett.*, **93**, 177401.
Tuinstra, F. and Koenig, J. L. (1970a), *J. Phys. Chem.*, **53**, 1126.
Tuinstra, F. and Koenig, J. L. (1970b), *J. Composite Materials*, **4**, 492.
Wang, F., Dukovic, G., Brus, L. E., and Heinz, T. F. (2005), *Science*, **308**, 838.
Wang, F., Sfeir, M. Y., Huang, L., Huang, X. M. H., Wu, Y., Kim, J., Hone, J., O'Brien, S., Brus, L. E., and Heinz, T. F. (2006), *Phys. Rev. Lett.*, **96**, 167401.
Zaric, S., Ostojic, G. N., Kono, J., Shaver, J., Moore, V. C., aand Robert H. Hauge, M. S. S., Smalley, R. E., and Wei, X. (2004), *Science*, **304**, 1129.
Zaric, S., Ostojic, G. N., Shaver, J., Kono, J., Portugall, O., Frings, P. H., Rikken, G. L. J. A., Furis, M., Crooker, S. A., Wei, X., Moore, V. C., Hauge, R. H., and Smalley, R. E. (2006), *Phys. Rev. Lett.*, **96**, 016406.
Zhang, Y., Tan, Y. W., Stormer, H. L., and Kim, P. (2005), *Nature*, **438**, 197.
Zhao, H. and Majumdar, S. (2005), *Synth. Met.*, **155**, 250.
Zhao, Y., Ando, Y., Liu, Y., Jinno, M., and Suzuki, T. (2003), *Phys. Rev. Lett.*, **90**, 187401.